

Attribution of the Seasonality and Regionality in Climate Trends over the United States during 1950–2000

HAILAN WANG

Goddard Earth Sciences and Technology Center, University of Maryland, Baltimore County, Baltimore, Maryland

SIEGFRIED SCHUBERT AND MAX SUAREZ

Global Modeling and Assimilation Office, NASA Goddard Space Flight Center, Greenbelt, Maryland

JUNYE CHEN

Earth System Science Interdisciplinary Center, University of Maryland, College Park, College Park, Maryland

MARTIN HOERLING

Climate Analysis Branch, NOAA/Earth System Research Laboratory, Boulder, Colorado

ARUN KUMAR AND PHILIP PEGION

Climate Prediction Center, NOAA/National Centers for Environmental Prediction, Camp Springs, Maryland

(Manuscript received 4 December 2007, in final form 10 November 2008)

ABSTRACT

The observed climate trends over the United States during 1950–2000 exhibit distinct seasonality and regionality. The surface air temperature exhibits a warming trend during winter, spring, and early summer and a modest countrywide cooling trend in late summer and fall, with the strongest warming occurring over the northern United States in spring. Precipitation trends are positive in all seasons, with the largest trend occurring over the central and southern United States in fall. This study investigates the causes of the seasonality and regionality of those trends, with a focus on the cooling and wetting trends in the central United States during late summer and fall. In particular, the authors examine the link between the seasonality and regionality of the climate trends over the United States and the leading patterns of sea surface temperature (SST) variability, including a global warming (GW) pattern and a Pacific decadal variability (PDV) pattern.

A series of idealized atmospheric general circulation model (AGCM) experiments were performed forced by SST trends associated with these leading SST patterns, as well as the residual trend pattern (obtained by removing the GW and PDV contributions). The results show that the observed seasonal and spatial variations of the climate trends over the United States are to a large extent explained by changes in SST. Among the leading patterns of SST variability, the PDV pattern plays a prominent role in producing both the seasonality and regionality of the climate trends over the United States. In particular, it is the main contributor to the apparent cooling and wetting trends over the central United States. The residual SST trend, a manifestation of phase changes of the Atlantic multidecadal SST variation during 1950–2000, also exerts influences that show strong seasonality with important contributions to the central U.S. temperature and precipitation during the summer and fall seasons. In contrast, the response over the United States to the GW SST pattern is an overall warming with little seasonality or regional variation. These results highlight the important contributions of decadal and multidecadal variability in the Pacific and Atlantic in explaining the observed seasonality and regionality of the climate trends over the United States during the period of 1950–2000.

Corresponding author address: Dr. Hailan Wang, Global Modeling and Assimilation Office (UMBC/GEST), Code 610.1, NASA Goddard Space Flight Center, Greenbelt, MD 20771.
E-mail: hailan.wang@nasa.gov

1. Introduction

The observed climate trends over the continental United States during 1950–2000 exhibit distinct seasonality and regionality. Figure 1 shows, for example, the observed linear trends¹ of the seasonal mean surface air temperature and precipitation over the United States during 1950–2000. The surface air temperature (Fig. 1a) exhibits a prominent warming trend during winter and spring with the strongest warming occurring over the northern and western United States in spring. During summer, the strong warming trend retreats, and a modest cooling trend emerges over the southern and central United States. The cooling strengthens and expands, and covers almost the entire United States in fall. For precipitation, most of the United States experiences an increase for all the seasons except for a notable drying trend over the northwestern coastal United States during winter (Fig. 1b). The enhancement in precipitation occurs mainly over the central and southern United States. The positive trend is relatively steady from winter to summer but then increases substantially in fall.

The above results are summarized in Fig. 2, which shows the regional average of the linear trend of the surface air temperature over the continental United States and the regional average of the linear trend of precipitation over the central United States. While the annual mean surface air temperature and precipitation (the 14th bar) display general warming and wetting trends during 1950–2000, the linear trends of these two fields show distinct seasonal variations, as clearly illustrated by the spatially averaged results. The surface warming (Fig. 2a) trend is prominent from winter to early summer, achieving a maximum of 1.2 K in late winter and early spring. A cooling trend is present from late summer to fall with a peak amplitude of -0.3 K in early fall. The precipitation (Fig. 2b) trend is positive for all seasons. The amplitude of the precipitation trend is relatively steady from midwinter to summer with a weak peak in late spring and early summer. It then jumps markedly and reaches a maximum in fall. The remarkable precipitation increase in fall corresponds very well with the concurrent cooling trend in surface air temperature. We note that the seasonality based on a countrywide average (not shown) is consistent with that based on the regional average over the central United States for both surface air temperature and precipitation in the Climate Research Unit (CRU) observations. Similar results (not shown) are obtained based

on other observational datasets, for example, the Global Historical Climatology Network (GHCN) data.

While there is now considerable evidence for an important anthropogenic influence on annual mean surface temperature trends during the latter half of the twentieth century on continental and larger scales (Hegerl et al. 2007), trends on subcontinental scales such as those over the central United States, are less well understood. The regionality of the U.S. climate trends, particularly the lack of a warming trend over the central United States, has been investigated in several recent studies. Based on a set of atmospheric general circulation model (AGCM) experiments forced with observed time-varying SST, Robinson et al. (2002) pointed to the importance of tropical Pacific SSTs for an annual cooling trend over the east-central United States during 1951–97, though it was unclear to what extent the tropical Pacific SST changes are themselves related to natural variability and to what extent they are associated with global warming. In an analysis of the coupled models simulations that were part of the Intergovernmental Panel on Climate Change (IPCC) Fourth Assessment Report (AR4) (2007) and were subjected to the observed evolution of the external forcing, Kunkel et al. (2006) found that, in contrast to the observed cooling trend over the central United States, warming trends occurred throughout the annual cycle in the coupled simulations. Furthermore, they suggest that internal ocean–atmosphere variability may have played a major role in determining the surface temperature trends over the United States. The observed linear trend of annual precipitation over the United States was also not reproduced in most IPCC AR4 coupled runs (C.-T. Chen 2007, personal communication). Using a regional climate model, Pan et al. (2004) found that regional-scale land–atmosphere feedback processes may partly explain the observed “warming hole” in the central United States in the last 25 years of the twentieth century.

While the above studies have made some progress in understanding the nature of the surface temperature trends over the United States, the causes for the seasonality and regionality of the observed trends are still not entirely clear. In particular, the seasonality of the trends has not yet been systematically investigated. In addition, the causes of the seasonal and regional variations of the observed precipitation increase over the United States, particularly why the increase is largest in fall, remain unresolved.

This study extends the above studies by further investigating the causes of the *seasonality* and *regionality* of the observed climate trends of both surface air temperature and precipitation over the United States during 1950–2000, with a focus on the cooling and wetting

¹ The linear trend of a field over a certain time period is defined as the linear regression coefficient of the time series with respect to time, multiplied by the length of the time period.

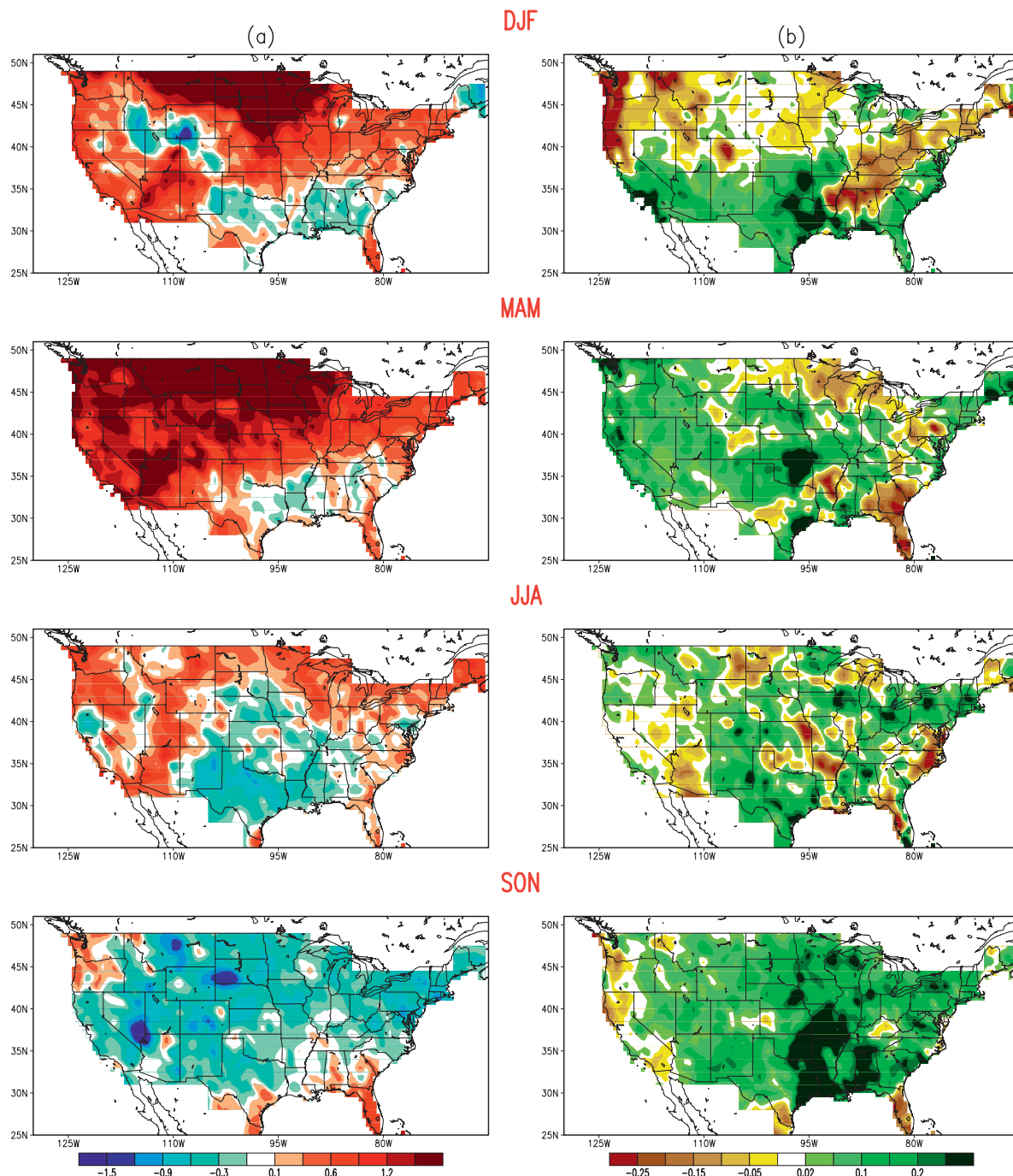


FIG. 1. Linear trends of (a) surface air temperature (K) and (b) precipitation (mm day⁻¹) over the United States during 1950–2000 for seasonal means over December–February (DJF), March–May (MAM), June–August (JJA), and September–November (SON). The data are from the dataset known as the CRU TS2.1 (Mitchell and Jones 2005).

trends in the central United States in late summer and fall. The premise of our analysis is that the observed U.S. trends during 1950–2000 are related to 1) trends in the SSTs (and to external forcing to the extent the SSTs trends are themselves forced), and 2) low-frequency

SST variability that is internal to the coupled ocean–atmosphere evolution and that also projects onto the U.S. trends.

As described in the next section, the linear trend of the observed SST over 1950–2000 is decomposed into

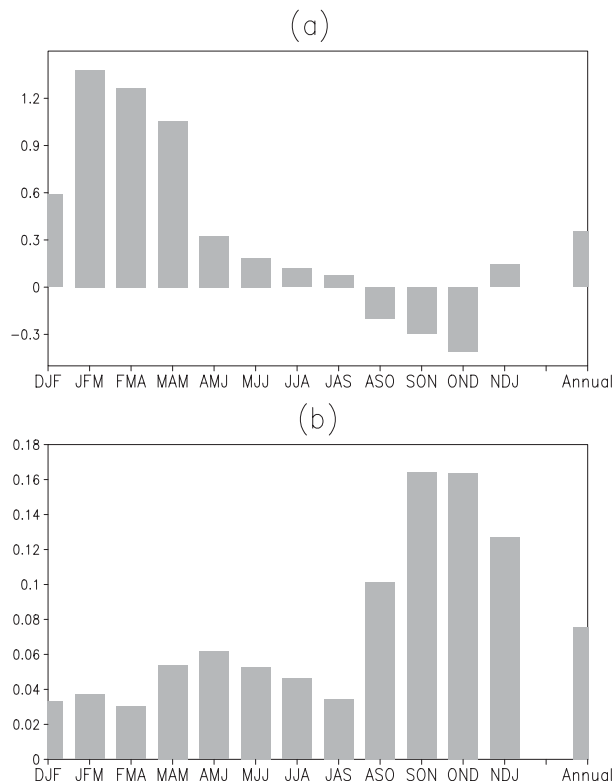


FIG. 2. Regional average of (a) the linear trend of surface air temperature (K) over the continental United States (25°–50°N, 235°–295°E) and (b) the linear trend of precipitation (mm day⁻¹) over the central United States (30°–48°N, 250°–275°E) during 1950–2000 for twelve 3-month running means and the annual mean (the 14th bar).

SST components associated with a global warming (GW) pattern, a Pacific decadal variability (PDV) pattern, and a residual pattern. By forcing the National Aeronautics and Space Administration (NASA) Seasonal-to-Interannual Prediction Project (NSIPP)-1 AGCM with various combinations of these SST anomalies both globally and over specific oceanic basins, this study examines to what extent the leading SST patterns explain the observed seasonality and regionality of surface temperature and precipitation trends over the United States during 1950–2000.

It is worth noting that the SST changes during 1950–2000 are a superposition of the internal variability on various time scales and the effects of both anthropogenic (e.g., greenhouse gases, aerosols, other man-made forcings) and natural external (e.g., changes in the solar irradiance and volcanic eruptions) climate forcings. Thus, the AGCM simulations to be discussed below implicitly include the effects of all of these external climate forcings to the extent that their influences are part of the observed SST time series.

Section 2 describes the observational datasets, the model output, the methodology used to obtain the lead-

ing SST empirical orthogonal functions, and the design of the AGCM experiments. In section 3 we examine and evaluate the AGCM simulations, and assess the relative roles of the leading SST EOFs in contributing to the observed seasonality and regionality of the climate trends over the United States. The summary and discussions are given in section 4.

2. Data and AGCM runs

a. Data

The surface air temperature and precipitation observations used here are part of the CRU TS 2.1 dataset, which is publicly available online (<http://www.cru.uea.ac.uk>; see Mitchell and Jones 2005). The data have a spatial grid of 0.5° latitude \times 0.5° longitude. We use monthly mean fields over the period 1950–2000. The CRU TS 2.1 data are consistent with the GHCN data in representing regional and seasonal variation of the U.S. climate trends (not shown), and the GHCN data are known reliable observational datasets for long-term climate trend detection (Solomon et al. 2007). We use the CRU TS 2.1 data in this study mainly because of its high spatial resolution. The observed SSTs are taken from the Hadley Centre Global Sea Ice and Sea Surface Temperature (HadISST) dataset (Rayner et al. 2003). The monthly mean HadISST data over the period 1901–2000 are used to compute various leading patterns (EOFs) of low-frequency SST variability and to provide lower boundary conditions for a series of idealized AGCM experiments described below.

b. NSIPP-1 AGCM and experiment design

For this study, the NSIPP-1 AGCM is run at horizontal resolution 3° latitude \times 3.75° longitude and 34 unequally spaced σ layers with high resolution (<200 m) in the lower 2 km of the atmosphere. The dynamical core of the model is described in Suarez and Takacs (1995). The boundary layer scheme is a simple K scheme, which calculates turbulent diffusivities for heat and momentum based on Monin–Obukhov similarity theory (Louis et al. 1981). The AGCM uses the relaxed Arakawa–Schubert (RAS) scheme to parameterize convection (Moorthi and Suarez 1992). The parameterization of solar and infrared radiative heating is described in Chou and Suarez (1994, 2000). The mosaic model (Koster and Suarez 1996) is used to represent land processes. Vegetation is prescribed with a climatological seasonal cycle. Details of the NSIPP-1 model formulation and its climate are described in Bacmeister et al. (2000). The seasonal predictability of the model is described in Pegion et al. (2000) for boreal winter and in Schubert et al. (2002) for boreal summer.

TABLE 1. List of the idealized AGCM experiments.

Expt	SST
Control	SSTClim (monthly SST climatology over 1944–76)
Total	SSTClim + SSTA_Total (linear change of SST over January 1950–December 2000)
Global warming	SSTClim + SSTA_GW (linear change of SST associated with GW EOF)
Uniform warming	SSTClim + 0.32 K
PDV	SSTClim + SSTA_PDV (linear change of SST associated with PDV EOF)
PDV in Pacific	SSTClim + SSTA_PDV_Pac (linear change of SST associated with PDV in Pacific)
Residual	SSTClim + SSTA_Residual (SSTA_Total – SSTA_GW – SSTA_PDV)
Residual in Atlantic	SSTClim + SSTA_Residual_Atl (linear change of residual SST in Atlantic)

A number of long model simulations are used to evaluate the performance of the NSIPP-1 AGCM in simulating the observations, as well as for comparisons with a series of idealized NSIPP-1 AGCM runs forced by the leading low-frequency SST EOFs. The long simulations, described in Schubert et al. (2004), consist of an ensemble of fourteen 104-yr (1902–2005) runs forced by observed monthly SSTs. These runs differ from one another only in their initial conditions. The concentration of CO₂ is fixed at the modern level, that is, 350 ppm. We focus here on the monthly mean surface air temperature and precipitation for the period 1950–2000.

The SST anomalies for the series of idealized AGCM experiments are obtained using the monthly Hadley SST over 1901–2000. The 100 years of SST data allow us to capture robust signals of natural long time-scale variations, such as the PDV. Since we are primarily interested in the low frequency signals that contribute to the recent trends, we first linearly remove the higher frequency El Niño–Southern Oscillation (ENSO) SST signal at each grid point using a maximum lead–lag cross-correlation analysis, described in Chen et al. (2008a).

The two leading EOFs (after removing the ENSO signal) consist of a general warming pattern [referred to as the global warming (GW) pattern] and a Pacific decadal variability pattern (Chen et al. 2008a,b; see section 3b). The linear trend of SST for the period 1950–2000 is then decomposed into the trends associated with the principle components (PCs) of the first two EOFs, as well as a residual trend computed as the difference between the full linear trend and the sum of the trends associated with the two leading PCs. Given that the linear trend of the observed SST does not exhibit any distinct month-to-month variations, all of the aforementioned linear trends are computed over January 1950–December 2000, and thus any seasonality of the SST trends is excluded.

We first carry out a control run forced with a SST climatology that is computed for the years 1944–76, a period during which the global mean SST does not exhibit any significant trends. In an anomaly run, the specified SST is the sum of the monthly SST climatology (1944–76) and the linear trend of SST over 1950–2000

associated with one of the leading SST EOFs. Note that the SST climatology varies from month to month, whereas the SST anomaly is fixed throughout the entire integration. To ensure a robust response, all AGCM runs are integrated for 100 years. The climatology of the runs is obtained by averaging the data over the last 60 yr. Note that the choice of averaging over 60 yr is rather arbitrary; averaging over any other time periods longer than 50 yr yields similar results. The difference between the control run and the anomaly run is used to represent the effect of the corresponding SST trend.

The idealized AGCM experiments are listed in Table 1: they include the control run, and anomaly runs forced with the full (1950–2000) linear trend of SST, the linear trends associated with the GW EOF and the PDV EOF, and the residual trend, over the global domain. To determine the regional SST anomalies that have dominant influences over the United States, we performed additional anomaly runs in which the AGCM is forced with the leading SST EOFs and the residual trend over specific ocean domains. They include the PDV EOF in the Pacific only (60°S–60°N), the residual trend in the Atlantic only (60°S–75°N), and the residual trend in the Indian (60°S–30°N) and Pacific (60°S–60°N) Oceans. In addition, to evaluate the importance of the *spatial pattern* of the SST anomalies associated with the GW EOF for the seasonality and regionality of the climate trends over the United States, we also perform an experiment in which the model is forced with a uniform SST warming of 0.32 K. The value of 0.32 K is the latitude-weighted average of the SST trend over 1950–2000 associated with the GW EOF between 60°S and 60°N.

3. Results

a. AMIP simulations

Figure 3 shows the 1950–2000 linear trends of the ensemble mean seasonal-mean surface air temperature and precipitation over the United States computed from the NSIPP-1 Atmospheric Model Intercomparison Project (AMIP) simulations. The comparison of the climate

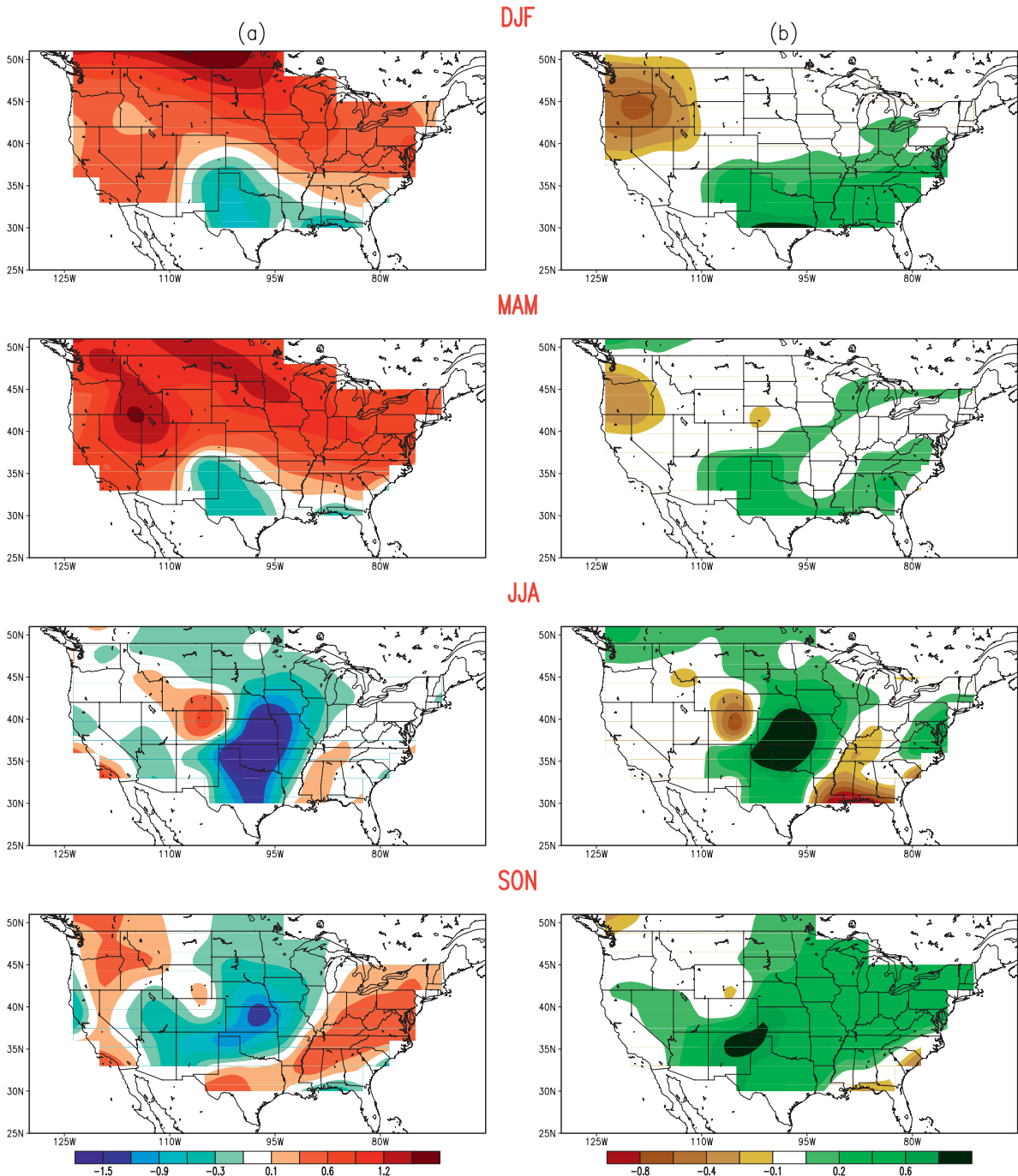


FIG. 3. Ensemble mean linear trends of seasonal mean (a) surface air temperature (K) and (b) precipitation (mm day^{-1}) over 1950–2000 in the NASA NSIPP-1 AMIP simulation for DJF, MAM, JJA, and SON. Note the use of a larger color scale for precipitation in Fig. 3 relative to that in Fig. 1.

trends in the simulations with those in the CRU observations (Fig. 1) shows general consistency. In particular, both simulated and observed surface air temperature show a prominent warming trend in the central and northern United States in winter and spring and a modest

cooling trend in the southern United States in spring. The warming trend is particularly strong and extensive during spring, with the maximum warming occurring over the northwestern United States and the northern plains. During summer, a strong cooling trend emerges

and dominates over the central United States, with weak regional warming to the west and east. During fall, the strong cooling trend over the central United States weakens slightly, shifts southwestward, and is surrounded by significant warming trends in the southeast and northwest portions of the United States.

The linear trend of simulated precipitation (Fig. 3b) corresponds well with that of surface air temperature (Fig. 3a), with an opposite sign, especially during the warm season. Qualitatively consistent with the CRU observations, the simulated wintertime precipitation shows a notable reduction over the northwestern United States, and a significant enhancement in the southern and southeastern coastal United States. In spring, the drying trend over the northwestern United States weakens notably, whereas the precipitation increase in the southern United States expands farther northward. During summer, a distinct precipitation enhancement occurs over the central United States, sandwiched between weak drying trends to the west and east. There are regional wetting trends along the east coast as well as the northern boundary of the United States. During fall, the majority of the United States experiences increasing precipitation, with the maximum increase occurring over the southwestern United States.

The comparison between the model simulations (Fig. 3) and the observations (Fig. 1) also shows some notable differences. In general, the spatial distribution of the climate trends over the United States in the AMIP ensemble mean simulation is much more systematic and organized than that in the CRU observations. This is mainly because the 14-member ensemble mean filters out the interensemble member noise and emphasizes the signals forced by the SST. The relationship between surface air temperature and precipitation trends is much smoother in the simulation than in the CRU observations. In addition, the simulated climate trends of surface air temperature and precipitation during the summer and fall months tend to be more localized and have their maximum centers located to the east and/or southeast of the Rockies, instead of farther east as shown in the observations. Also, the amplitudes of the cooling and wetting trends in the model simulation are substantially stronger than those in the observations (note the use of different color scales). This likely reflects an overall wet bias in the model's precipitation climatology (e.g., Lee et al. 2007). Despite these differences, we conclude that the basic features of the seasonality and regionality of the observed climate trends over the United States are generally well reproduced in the model ensemble-mean simulations.

The seasonality of the climate trends over the United States in the NSIPP-1 AMIP runs and the comparison to the CRU observations are more clearly illustrated in

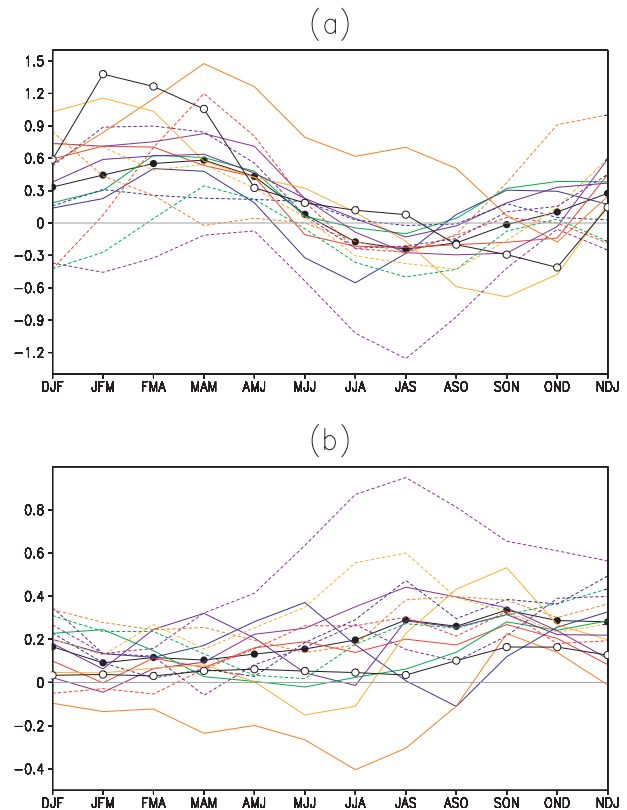


FIG. 4. Regional average of (a) the linear trend of surface air temperature (K) over the continental United States (25° – 50° N, 235° – 295° E) and (b) the linear trend of precipitation (mm day^{-1}) over the central United States (30° – 48° N, 250° – 275° E) during 1950–2000 for twelve 3-month running means, for each of the 14 members (thin colored lines), the 14-member ensemble mean (thick black line with close circle) in the NSIPP-1 AMIP simulations, and the CRU TS2.1 observations (thick black line with open circle).

Fig. 4, which shows the regional average of the linear trend of surface air temperature over the United States, and that of precipitation over the central United States. The regional average over the central United States, instead of the entire continent, for precipitation is chosen mainly because, unlike for the observations, there is a strong cancellation when averaging the model precipitation trend over the continental United States. Figure 4 clearly demonstrates the general similarity of the trends in the NSIPP-1 AMIP ensemble simulations and the CRU observations. The CRU observations fall within the spread of the NSIPP-1 ensemble simulations except for surface air temperature during late winter and early spring when the CRU observations show somewhat stronger warming. Similar to what is found for the CRU observations, the simulated surface warming trend (Fig. 4a) is present from winter to early summer, achieving its maximum intensity in late winter and early spring, whereas a

notable cooling trend is present in late summer and fall months, peaking in late summer. Despite considerable intraensemble variability, most of the 14 ensemble members show increasing precipitation trends throughout the seasonal cycle, with the peak increase occurring in late summer and early fall (Fig. 4b). There are some notable differences between the ensemble mean simulation and the observations, particularly in terms of the amplitude of the climate trends. The ensemble mean simulation significantly underestimates the magnitude of the observed warming in winter and early spring, yet overestimates the observed precipitation enhancement for all seasons. The simulated cooling amplitude in late summer and fall is somewhat stronger than that in the observations. Meanwhile, the amplitude of the precipitation increase in the model simulation is at least twice as strong as that in the observations for all seasons.

We conclude from the above results that the NSIPP-1 model, when forced with the observed SSTs, provides a reasonably good simulation of the seasonality and regionality of the observed climate trends over the United States. The agreement between the NSIPP-1 ensemble mean simulation and the observations highlights the importance of the SST in forcing the observed spatial and temporal distribution of climate trends over the United States. Other factors, such as the direct effects of external radiative forcings, coupled ocean–atmosphere processes, observed trends of internal atmospheric variability (e.g., Arctic Oscillation), land use change, and changes in sea ice, while potentially important, are not included in the AMIP simulations. We note, however, that Robinson et al. (2002) found that the annual mean cooling over the east-central United States is present in their AGCM runs forced by observed varying SST, regardless of whether the increasing greenhouse gases and other time-varying climate forcings are included. In the following, we look in more detail at the role of SSTs in forcing the seasonal and regional variations of the trends in the U.S. surface air temperature and precipitation. We begin by examining the 1950–2000 linear SST trends associated with the leading low-frequency SST EOFs.

b. Leading SST patterns

Figure 5 displays the spatial distribution and temporal evolution of the two leading EOFs of the monthly Hadley SST (with ENSO linearly removed, see section 2b). On the basis of their temporal evolution and spatial structure, which are detailed below, these two EOFs are referred to as the GW and PDV patterns, respectively (Chen et al. 2008a,b). The GW and PDV EOFs explain 30% and 12% of the monthly SST variance, respectively. The GW EOF (Fig. 5a) exhibits a general warming trend over most of the oceanic regions. The largest warming

occurs in the Indian and Atlantic Oceans, whereas the Pacific exhibits the weakest warming among the major ocean basins. In addition, the SST warming in the extratropics is stronger than that in the tropics. The time series of the associated PC of the GW EOF (Fig. 5b) is similar to the long-term change of global mean surface temperature (Houghton et al. 2001). It is characterized by a significant increase in the 1930s, a leveling off from the early 1940s to 1976, and a more pronounced warming trend afterward.

The distribution of the PDV EOF (Fig. 5c) is consistent with that revealed in numerous previous studies based on various statistical analyses (e.g., Zhang et al. 1997). In the warm phase, it is characterized by strong warm SST anomalies in the central and eastern tropical Pacific and distinct cooling in the North Pacific along 40°N and the oceanic regions to the east and southeast of Australia. There is a weak warming in the SH subtropical Indian Ocean as well. The SST anomalies in the Atlantic Ocean are generally small by comparison. In contrast with the GW EOF where the main SST changes occur in the Indian and Atlantic Oceans, the major warming and cooling centers in the PDV EOF occur in the Pacific. Moreover, from a zonal mean perspective, the PDV EOF shows a strong tropical warming and a cooling trend in the extratropics. The time series of the PC of the PDV pattern (Fig. 5d) displays a positive phase prior to the early 1940s, a phase change around 1944, a negative phase from 1944 to 1976, and then a distinct phase shift around 1976–77, followed by a positive phase afterward. We note that the GW and the PDV EOFs obtained using the Hadley SST are similar to those computed from the Extended Reconstructed SST (ERSST) and the NASA Goddard Institute for Space Studies (GISS) Surface Temperature Analysis (GISTEMP) data described in Chen et al. (2008a,b). A detailed examination and discussion of the GW and the PDV EOFs is given in Chen et al. (2008a,b).

Figure 6 shows (a) the total linear trend of the Hadley SST, (b) the SST trend associated with the GW EOF, (c) the SST trend associated with the PDV EOF, and (d) the residual SST trend for the period from January 1950 through December 2000. The total linear trend (Fig. 6a) is characterized by an El Niño–like change in the Pacific, a strong warming trend in the Indian Ocean, and a notable warming over the Southern Hemisphere (SH) Atlantic Ocean. In contrast, the North Atlantic is covered by regional cooling off the southeast coast of the United States, the tropical Atlantic, and the extratropical Atlantic along 60°N. The distributions of the GW (Fig. 6b) and the PDV (Fig. 6c) patterns are the same as those in Fig. 5 except that they show the amplitude of the linear trends of the SST anomalies associated with these two EOFs over the period 1950–2000.

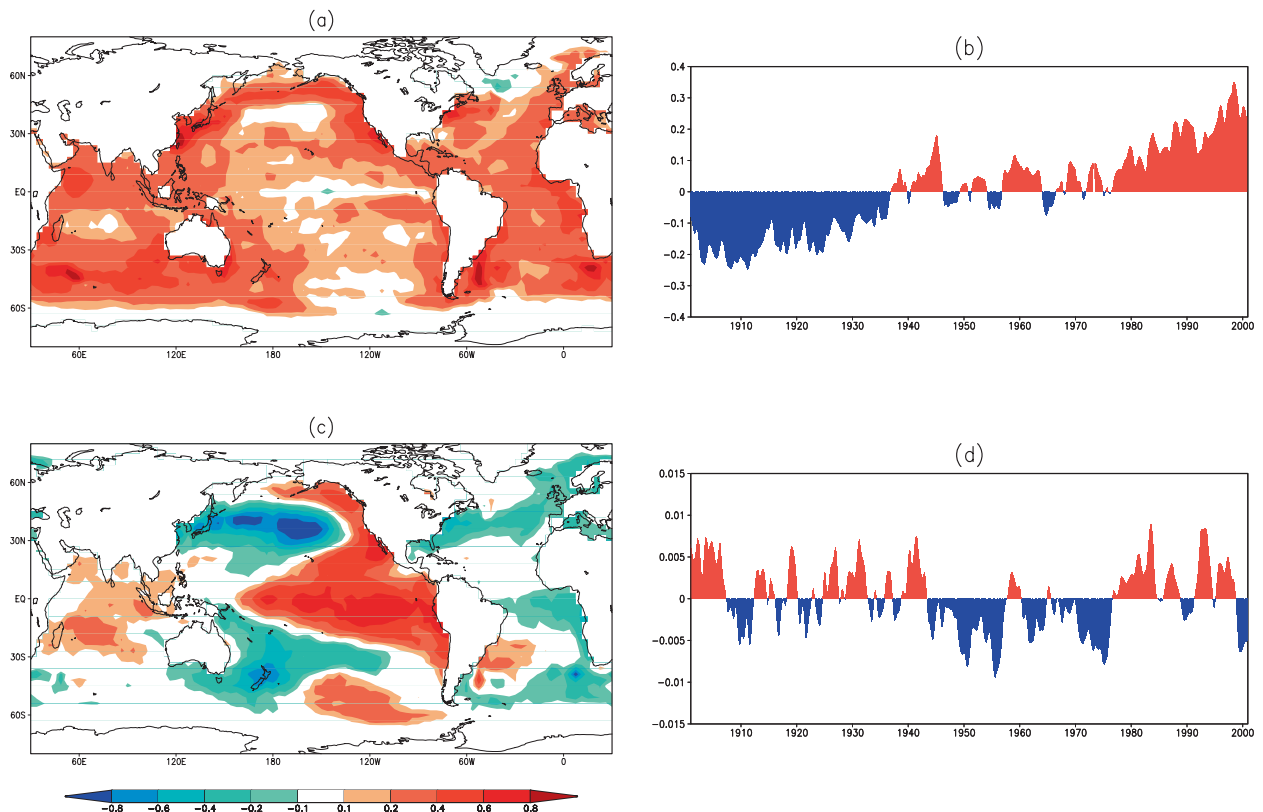


FIG. 5. Spatial distribution (K) of (a) the GW and (c) the PDV SST EOFs, and the time series of (b) the GW and (d) the PDV SST EOFs. The analysis is performed using the monthly HadISST over January 1901–December 2000.

The residual SST trend (Fig. 6d) exhibits regional cooling over the Atlantic including a strong cooling trend over the NH tropical Atlantic, a modest cooling off the southeast coast of the United States, and a strong cooling trend immediately south of Greenland and Iceland. There are moderate warming trends over the tropical Indian Ocean and the western Pacific, and regional coolings that are off the west coasts of the American continents. We note that the residual SST trend is basically the combination of the third (5.4%) and fourth (5.0%) EOFs of the monthly Hadley SST that has ENSO linearly removed (not shown). The features in the tropical and the NH Atlantic project strongly onto the third EOF, whereas the features in the other regions project onto the fourth EOF. The PC of the former resembles the Atlantic multidecadal variability (AMV) pattern (Enfield et al. 2001), though the nature of the residual SST trend is not entirely clear. The comparison among the four panels in Fig. 6 indicates that the SST trends in the Pacific, the Indian and SH Atlantic Oceans, and the NH Atlantic Ocean are dominated by the PDV EOF, the GW EOF, and the residual component, respectively. These linear trends of SSTs provide the inputs for the series of idealized AGCM experiments described next.

c. Contributions from the leading SST EOFs

Figure 7 shows the AGCM response of the surface air temperature to the linear SST trends associated with (a) the full SST, (b) the GW EOF, (c) the PDV EOF, and (d) the residual SST field for each season. The comparison between the AGCM response to the specified linear trend in SST (Fig. 7a) and the trends obtained from the AMIP simulations (Fig. 3a) shows a striking similarity, with only small differences. In particular, the impact of having the full SST variability (inherent to the AMIP run) is to only modestly enhance the surface air temperature responses in winter and spring and contribute to additional cooling over the far western and eastern United States during summer and fall. Thus, our idealized AGCM experiments with fixed SST anomaly provide a useful framework for understanding the nature of the U.S. trends.

The relative contributions of the SST EOFs are revealed by comparing the AGCM response to the total linear trend of SST to those of the various leading SST EOFs. For all seasons, the AGCM response to the GW EOF (Fig. 7b) differs significantly from the response to the total trend in SST (Fig. 7a). The GW EOF mainly

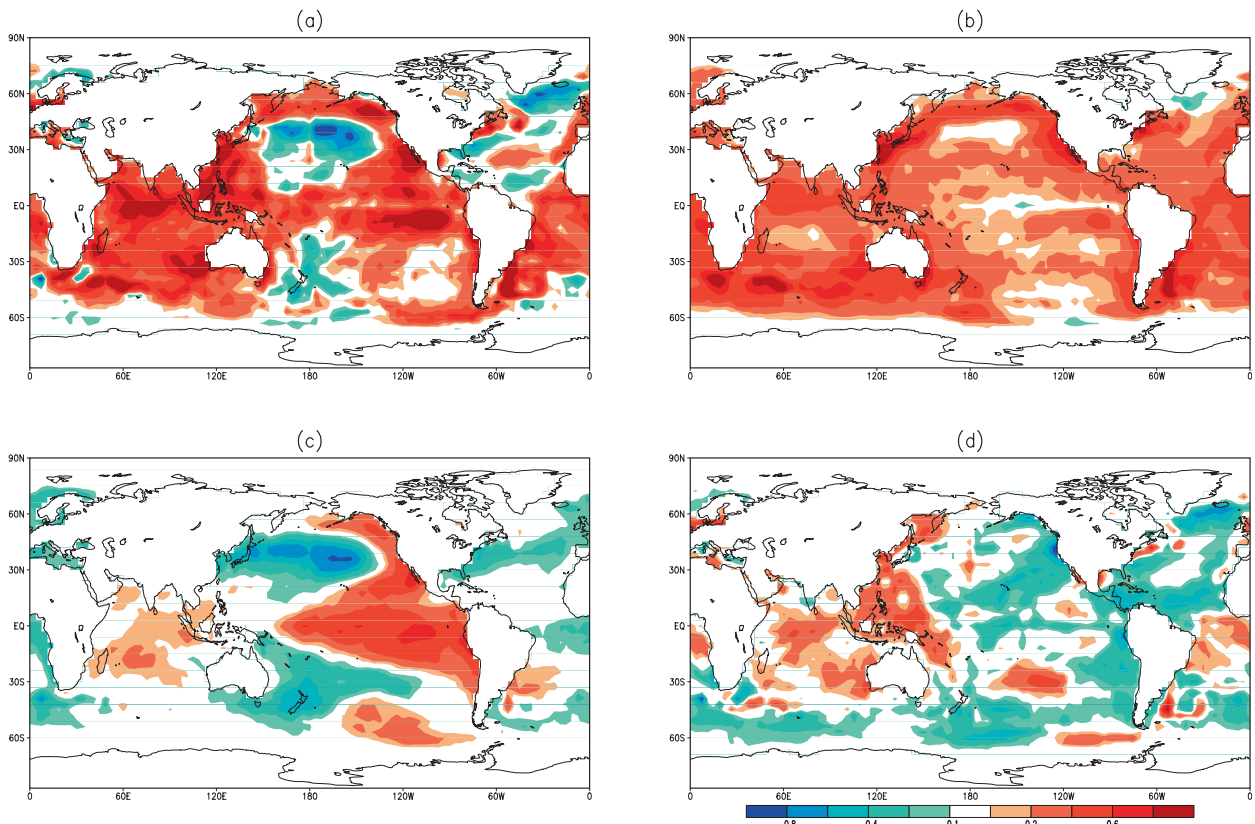


FIG. 6. Linear trends of (a) the HadISST, (b) the SST anomalies associated with the GW EOF, (c) the SST anomalies associated with the PDV EOF, and (d) the residual SST component (K), over January 1950–December 2000.

leads to a prominent warming over the entire country with the maximum warming generally present over the central United States. The spatial pattern does not resemble the AGCM response to the total trend in SST overall. In winter, the strongest warming response is over the Midwest and central United States. From spring to fall, the GW EOF forces a strong warming response over the central southern United States, in contrast with the AGCM response to the total linear trend which displays a distinct cooling trend. The main contribution of the GW EOF to the total trend appears to be the notable warming trends over the western and eastern United States during the summer and fall seasons.

In contrast with the GW EOF, the spatial pattern of the AGCM response to the PDV EOF (Fig. 7c) shows a considerable resemblance to that of the response to the total trend (Fig. 7a) for all seasons. Similar to the results shown in Fig. 7a, the PDV EOF forces a distinct warming response over the northern United States and a cooling trend farther south in winter and spring. Nevertheless, the amplitude of the warming trend appears to be the strongest in winter. The cooling over the southern United States is stronger and more spatially

extensive, especially in spring. During summer and fall, the PDV EOF forces a distinct cooling trend over the central United States. The cooling trend is slightly weaker yet more widespread in fall than in summer. There are, however, no significant warming responses on the west and east sides of the cooling response in summer and fall.

The response to the residual SST trend (Fig. 7d) is a general cooling trend throughout the seasonal cycle. During winter and spring, it mainly leads to a pronounced cooling trend over western and central United States and a warming response over eastern United States. During summer, it forces a distinct cooling trend over the central plains, though the response is weaker and less extensive compared to that produced by the PDV EOF. The cooling response extends westward in fall, with a modest warming response to the east.

Figure 8 is the same as Fig. 7 except for precipitation. The similarity of the precipitation response to the total linear trend of SST (Fig. 8a) and the trend from the AMIP ensemble mean simulation (Fig. 3b) is even greater than that for surface air temperature, emphasizing the secondary importance of any seasonal variations

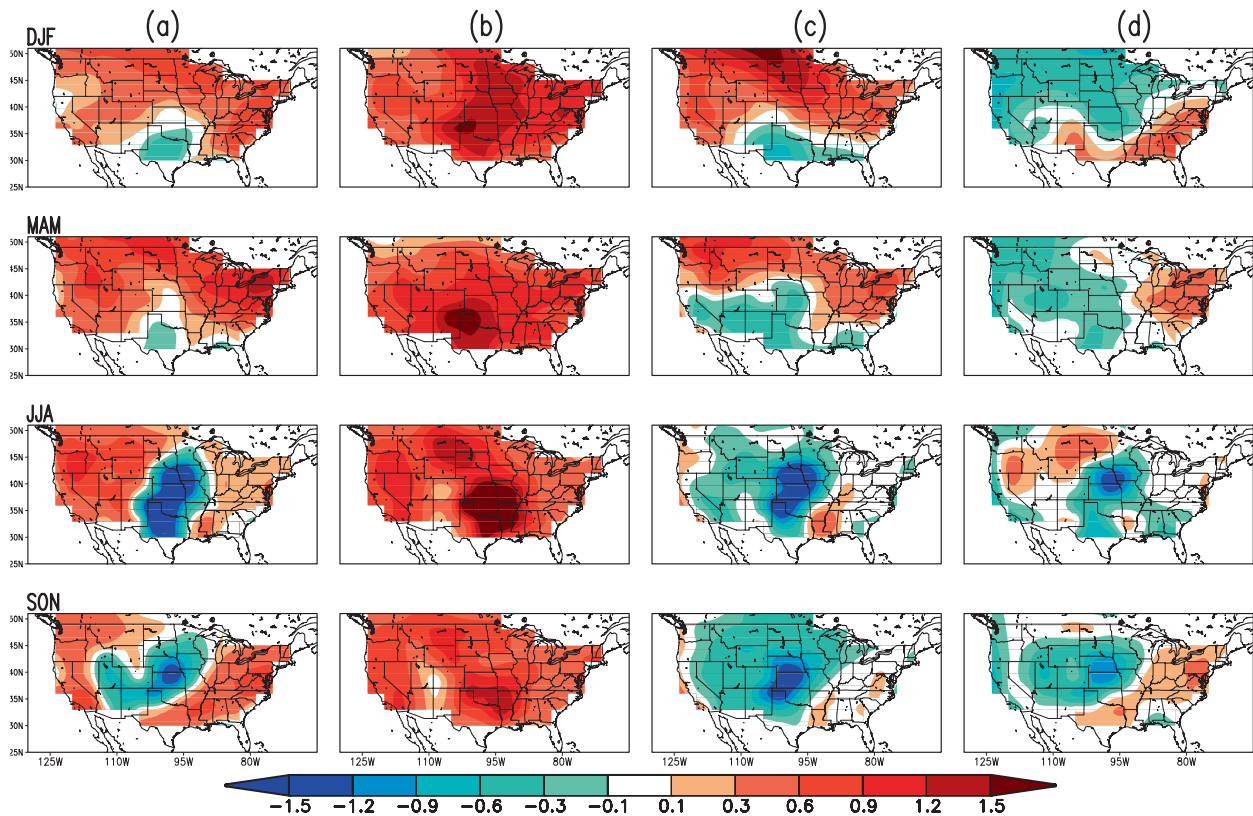


FIG. 7. Surface air temperature (K) in the AGCM responses to the linear trends of (a) the total SST, (b) the SST anomalies associated with the GW EOF, (c) the SST anomalies associated with the PDV EOF, and (d) the residual SST component, for DJF, MAM, JJA, and SON.

of the SST trend for the long-term changes of precipitation over the United States.

The relative roles of the leading SST EOFs in producing the trends of precipitation are similar to those for surface air temperature. For all seasons, the precipitation response to the GW EOF (Fig. 8b) is generally opposite to the response to the total trend in SST (Fig. 8a). Contrary to the general precipitation increase shown in Fig. 8a, the GW EOF forces wetting trends over the northwestern United States and drying trends over the southern United States in winter and spring. During summer and fall, there are drying responses over the southern and central United States, with wetting responses to the west. In contrast, the precipitation response to the PDV EOF (Fig. 8c) is consistent with the response to the total trend in SST in both spatial pattern and amplitude, particularly for summer and fall. The PDV EOF contributes to a modest precipitation reduction over the northwestern United States and a rainfall increase over the southwestern and southeastern United States in winter. In spring, the modest precipitation reduction over the northwestern United States persists, whereas the central and southern United States shows a precipitation increase.

During summer, similar to the response to total SST trend, the PDV EOF forces a distinct rainfall increase in the central United States to the east of the Rockies and modest drying trends to the east and southeast. The rainfall increase weakens somewhat, yet becomes more spatially extensive in fall, with the maximum precipitation increase centered over the southwestern United States. The residual SST trend makes a rather significant contribution to the precipitation trends over the United States in winter, summer, and fall as well. During winter, it contributes to the drying trend over the northwestern United States and the wetting trend over the southeastern United States. In summer, it forces a notable precipitation enhancement over the central plains surrounded by drying to the north and east. It also produces a widespread wetting trend that centers over the southwestern United States in fall. The precipitation responses to the residual SST trend in summer and fall are quite similar to the responses to the PDV EOF. The contribution by the residual SST trend is, however, somewhat weaker than that of the PDV EOF in summer, yet slightly stronger in fall.

To examine the relative roles of the leading SST EOFs in accounting for the *seasonality* of the climate

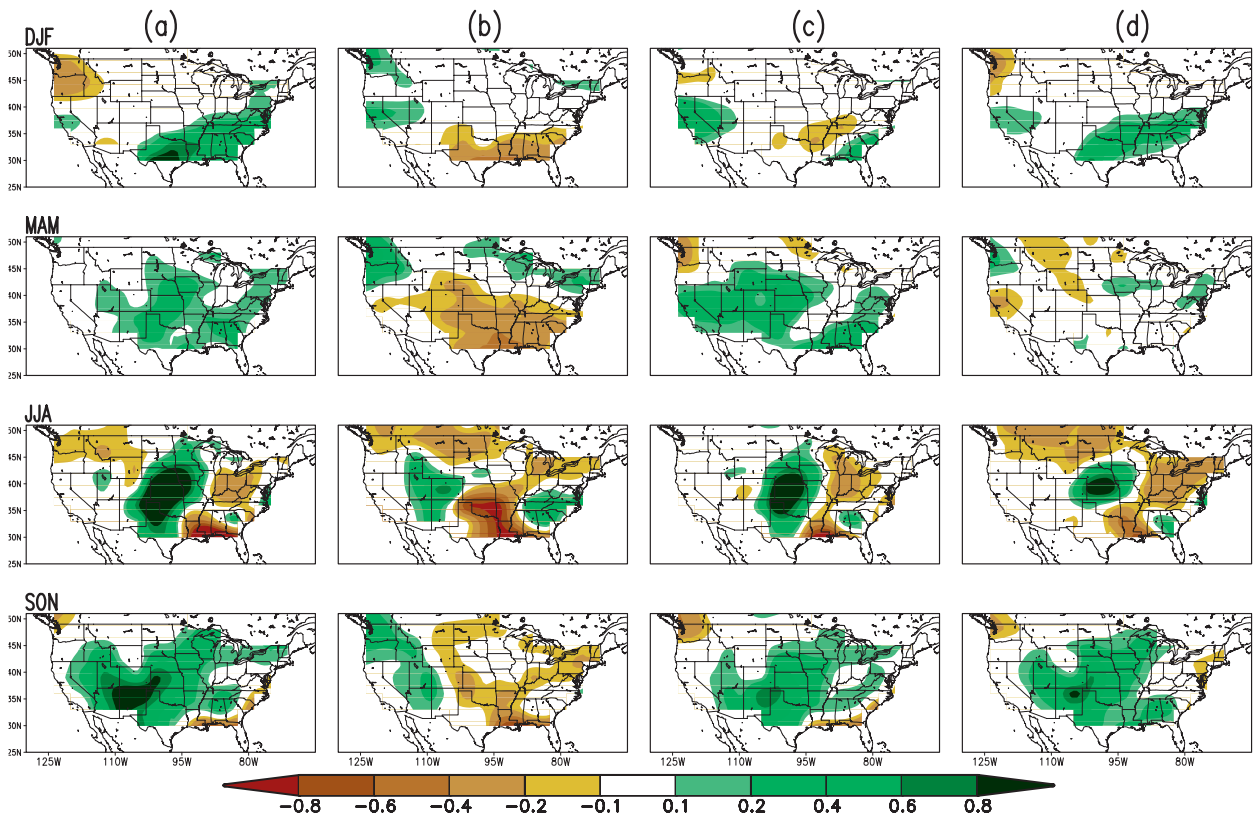


FIG. 8. As in Fig. 7 but for precipitation (mm day^{-1}).

trends over the United States, Fig. 9 shows the surface air temperature response averaged over the United States and the precipitation response averaged over the central United States. The results of the AGCM response to the Pacific component of the PDV EOF, the Atlantic component of the residual SST trend, and the uniform SST warming of 0.32 K are also included in Fig. 9 for comparison. The AGCM response to the total trend in SST is in good agreement with the AMIP ensemble mean simulation, especially for precipitation. The agreement between the AMIP and the AGCM response to the total trend in SST over the central United States is above the 95% statistical significance for both surface air temperature and precipitation for all seasons (not shown). Similar to the AMIP simulation, the AGCM response to the total trend in SST exhibits the maximum warming in spring and a cooling trend in late summer and early fall. The precipitation response shows a significant increase for all seasons with the strongest increase occurring in late summer and fall. However, the maximum warming in the response to the total trend in SST occurs in spring instead of late winter and early spring in the AMIP simulations. Moreover, during summer and fall, owing to stronger cancellation between the cooling trend over the central United States

and the warming trends in surrounding regions in the AGCM response to the total SST trend (Fig. 7a), the continental U.S. mean cooling trends are not as strong as those in the AMIP simulation.

Figure 9 also shows that the GW EOF contributes to a significant continental-mean warming of 0.8 K and a drying trend that persists throughout all seasons. The uniform SST warming of 0.32 K also leads to a general warming and drying response over the United States for all seasons, though the warming and drying amplitudes are considerably weaker than those for the GW EOF. The general similarity between the AGCM response to the GW EOF and that to the uniform warming indicates that the details in the spatial pattern of the GW EOF are of secondary importance; they mainly contribute to a modest warming and drying. In contrast, the AGCM response to the PDV EOF resembles that of the response to the total SST trend. The PDV EOF forces a warming trend from winter to early spring and a cooling trend from late spring to fall, with the strongest warming and cooling trends occurring in winter and fall, respectively. The PDV EOF forces a notable precipitation increase for almost all seasons, the seasonality of which is qualitatively similar to that of the response to the total SST trend in that the maximum precipitation increase occurs

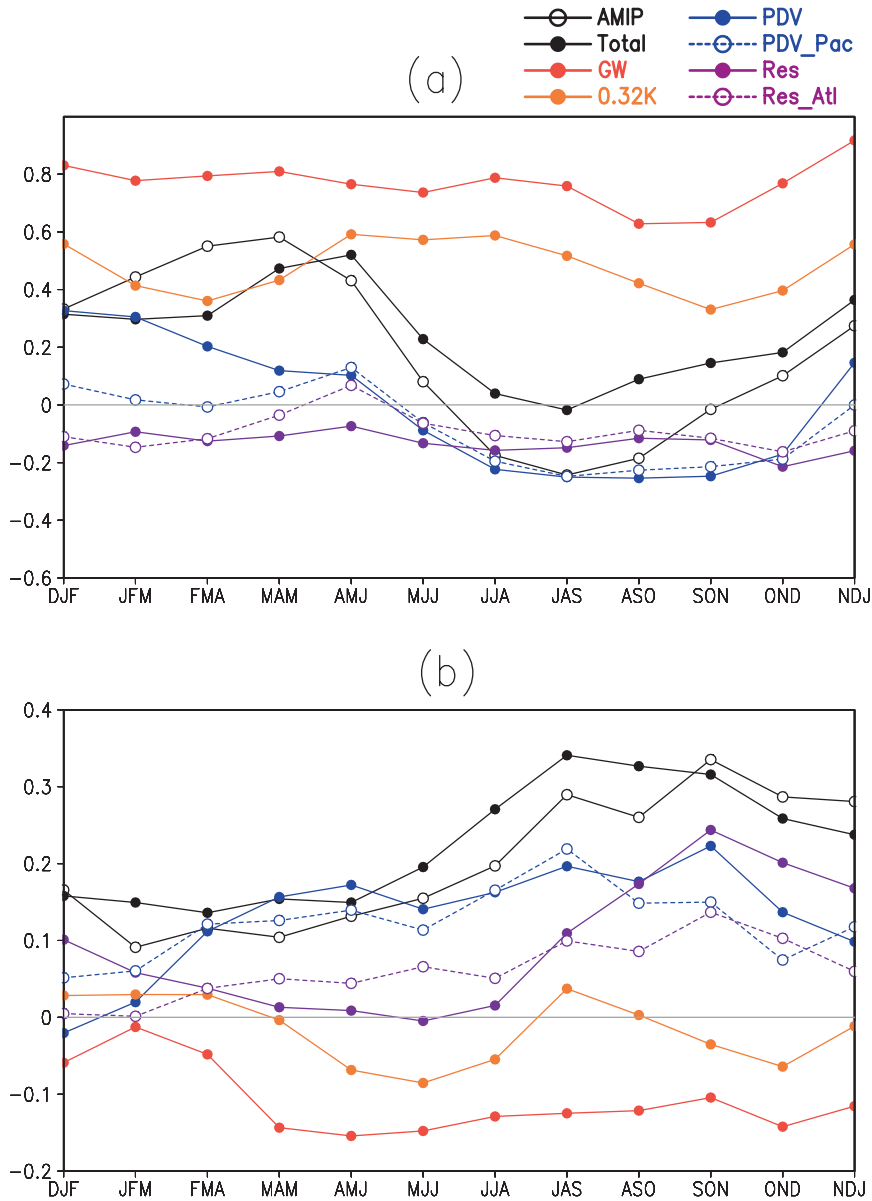


FIG. 9. Distribution of (a) the surface air temperature (K) response averaged over the United States, and (b) the precipitation (mm day^{-1}) response averaged over the central United States, for twelve 3-month running means, in the NSIPP-1 AMIP ensemble mean simulation (black line with open circle), the AGCM response to the total trend in SST (black line with close circle), and the AGCM responses to the SST trends associated with leading SST EOFs over global and specific ocean domains (colored lines).

in fall. Nevertheless, while the increase of precipitation in spring is comparable to that in the AGCM response to the total SST trend, the PDV EOF accounts for only about half of the precipitation increase in the AGCM response to the total SST trend during summer and fall.

The comparison in Fig. 9 between the responses to the PDV EOF and to the Pacific-only part of the PDV shows strong similarities for all seasons except winter

and early spring when the PDV EOF over the global domain shows a stronger warming. This suggests that the effect of the PDV EOF on the climate of the United States mainly comes from the Pacific. The SST anomalies associated with the PDV EOF in other oceanic basins mainly contribute to additional warming in winter and early spring. In contrast to the GW and the PDV EOFs, the residual SST trend leads to a country mean

cooling of -0.18 K that persists throughout the year. Its contribution to the enhanced precipitation over the central plains is relatively insignificant from late winter to midsummer and then increases dramatically in late summer, reaches a peak in late fall, and gradually declines afterward. The AGCM response to the Atlantic-only residual SST trend shows a strong similarity to the response to the residual SST trend for all seasons, indicating that the influence of the residual SST mainly comes from the Atlantic. It is noteworthy that the precipitation enhancement forced by the residual SST trend is modestly stronger than that forced by the PDV EOF in late fall and early winter. The effects of the PDV EOF and the residual SST trend combine to give the maximum wetting trend in fall. In addition, we note that, while the nonlinearity in the AGCM responses is noticeable, it is below the 90% statistical significance for the regional mean surface air temperature for all seasons and precipitation for most seasons (not shown). Moreover, an inspection of the spatial maps of the responses shows that the nonlinearity is primarily in the amplitude, not in the spatial pattern of the responses. Thus, any nonlinearity that exists does not affect our main conclusions.

To compare the *spatial pattern* of the trends over the United States among the various AGCM runs, Fig. 10 shows the spatial pattern correlation between the AGCM response to the linear trend of total SST and other AGCM simulations, including the idealized AGCM runs and the NSIPP-1 AMIP ensemble mean simulation, over the continental United States. Figure 10 clearly illustrates the rather high spatial pattern correlations between the AGCM response to the linear trend of total SST and the trends in the NSIPP-1 AMIP ensemble mean simulation for both surface air temperature (Fig. 10a) and precipitation (Fig. 10b) throughout the seasonal cycle, and thus highlights the inconsequential role of any seasonality of the SST forcing in contributing to the spatial pattern of the trends over the United States. The AGCM response to the GW EOF has rather low correlation for surface air temperature and notably negative correlation for precipitation for most seasons, emphasizing the secondary role of the GW EOF in contributing to the spatial pattern of the climate trends over the United States. The insignificant pattern correlation for the uniform warming indicates that the general SST warming is unimportant for the spatial pattern of the U.S. climate trends. In contrast, the AGCM response to the PDV EOF exhibits rather high spatial pattern correlation for both surface air temperature and precipitation, particularly in summer and fall months. This further stresses the importance of the PDV EOF in contributing to the spatial pattern of the climate trends over the United States, especially in summer and fall. The correlation for the PDV

EOF limited to the Pacific is generally consistent with that for the PDV EOF (over the global domain), though with a slightly lower value, again suggesting that the effect of the PDV EOF mainly comes from the Pacific. The contribution by the residual SST component is notable. The correlation for surface air temperature is generally low during winter and spring and then jumps to a value as high as 0.7 in late summer and fall. The pattern correlation for precipitation is also high (>0.6) for all seasons except early spring. The correlation for the residual SST component is even slightly higher than that for the PDV EOF in winter and late summer. For both surface air temperature and precipitation, the pattern correlations for the residual trend limited to the Atlantic exhibit strong similarity to those for the residual trend over the global domain. This highlights the significance of the residual SST component, particularly that in the Atlantic, in forcing the spatial pattern of the cooling and wetting trends over the central United States in late summer and fall.

The above comparison of the AGCM response to the total trend in SST and the responses to the leading SST EOFs in Figs. 7–10 indicates that the PDV EOF, particularly the SST anomalies in the Pacific, plays a leading role in producing the climate trends in both amplitude and spatial pattern for all seasons. In contrast, the GW EOF mainly forces a general warming and drying trend throughout the seasonal cycle. This is partially offset by the response to the residual SST trend, which consists of a cooling trend for all seasons, and a significant enhancement in precipitation over the central United States in late summer and fall. The precipitation increases over the central United States forced by the PDV EOF and the residual SST trend peak in summer and fall, respectively. The distinct wetting trend over the central United States during summer is mainly forced by the PDV EOF and, to a lesser extent, also by the residual trend, whereas the strong precipitation enhancement in fall is comparably maintained by both. Additional AGCM experiments forced by residual SST trends limited to various subregions of the Atlantic (not shown) show that the response to the residual SST over the United States is mainly explained by the SST cooling trend over the NH tropical Atlantic, a manifestation of the phase changes of the AMV during the period 1950–2000.

4. Summary and discussions

The observed trends of surface air temperature and precipitation over the United States during 1950–2000 exhibit distinct seasonality and regionality. This study uses the NASA NSIPP-1 AGCM to investigate the causes of these trends, particularly the cooling and wetting trends

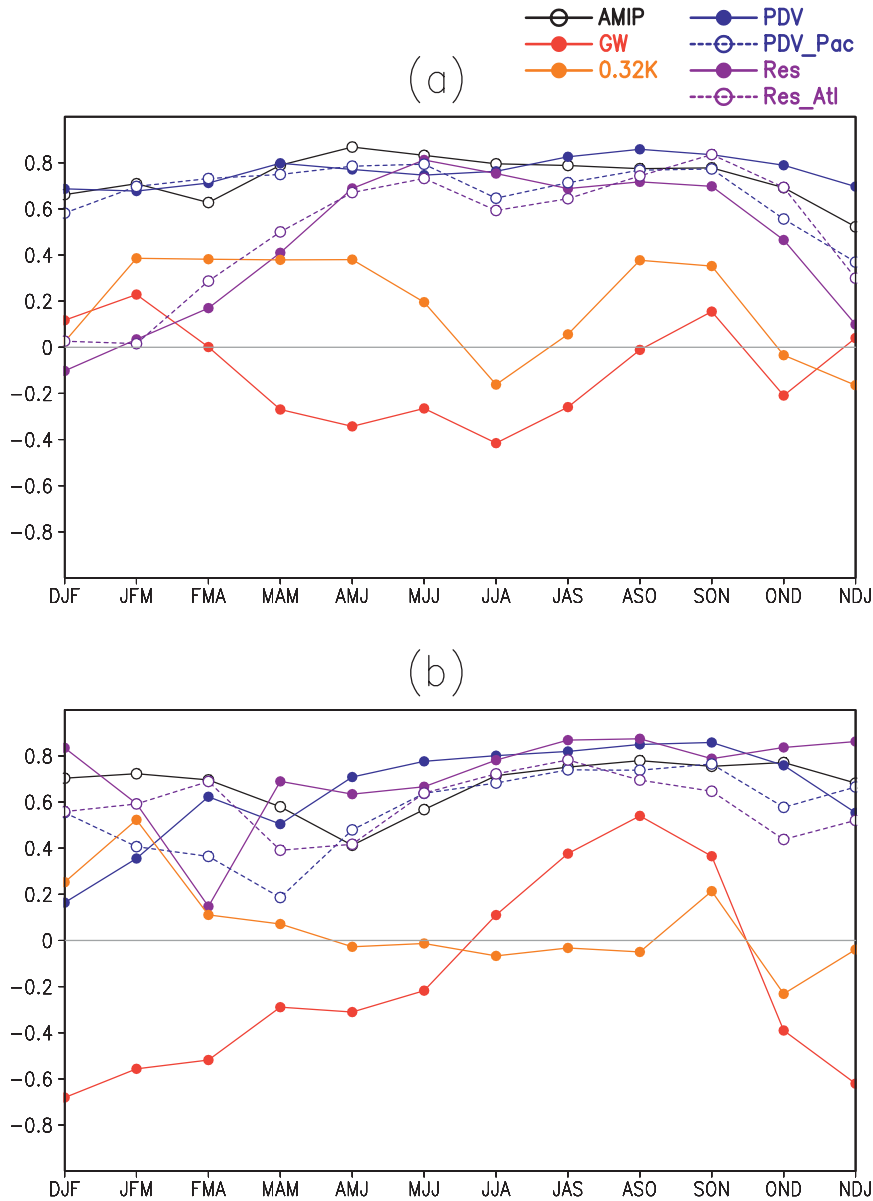


FIG. 10. Spatial pattern correlation between the AGCM response to the total trend in SST, and other AGCM simulations including the NSIPP-1 AMIP ensemble mean simulation (black line with open circle) and the AGCM responses to the SST trends associated with leading SST EOFs over global and specific ocean domains (colored lines), over the continental United States, for (a) surface air temperature and (b) precipitation, for twelve 3-month running means.

in late summer and fall. From model simulations forced with the observed SST we find that the seasonality and regionality of the 1950–2000 observed climate trends over the United States can, to a large extent, be explained by the changes in SST. This relationship is further explored by forcing the model with the trends associated with the leading patterns of SST variability consisting of a GW pattern, a PDV pattern, and a residual pattern.

The results of the model simulations show that, among the leading low-frequency SST EOFs, the PDV EOF in the Pacific plays a prominent role in forcing the spatial and seasonal variations of the climate trends over the United States throughout the seasonal cycle. The residual SST trend in the NH tropical Atlantic, a reflection of the influences of the AMV, makes a comparable contribution to the cooling and wetting trends during fall. In contrast, the SST changes associated with

the GW EOF mainly provide a general warming and drying response over the continental United States. In fact, the effect of the GW EOF is similar to that of a uniform oceanic warming, as one might expect from greenhouse gases, the distribution and influence of which are mainly uniform (Houghton et al. 2001; Solomon et al. 2007). In summary, our results highlight the essential importance of decadal variability for understanding the seasonal and regional variations of the climate trends over the United States during the period 1950–2000.

The importance of the PDV for explaining the regional variations of the U.S. climate trends revealed in this study is consistent with Robinson et al. (2002). That study, using a different AGCM (the NASA GISS model), found that the annual cooling trend over the east-central United States during 1951–97 is largely tied to the low-frequency SST changes in the tropical Pacific. As a further assessment of model dependence of our results, we have also examined the 1950–2000 AMIP simulations made with the National Center for Atmospheric Research (NCAR) Community Climate Model 3 (CCM3) (Kiehl et al. 1998; Seager et al. 2005) and the GFDL AM2.0 (Delworth et al. 2006) models (not shown). The results from those runs regarding the seasonality and regionality of the U.S. climate trends (not shown) are in general agreement with the current study. The main difference is in the seasonality; the strongest cooling and wetting trends occur in summer for the NCAR CCM3 and in late spring and early summer for the GFDL AM2.0. In that regard, the late summer and fall cooling and wetting trends in the NASA NSIPP-1 model appear to be more faithful to the observations. The general agreement between the three models and the observations further supports the important role of SST for the observed climate trends over the United States during 1950–2000.

While we highlight the importance of decadal variability in determining the seasonal and regional characteristics of the U.S. precipitation and surface temperature trends, our results do not contradict past studies that have focused primarily on the area-mean annual mean trends over continental and larger-scale regions. In particular, they are not inconsistent with the IPCC results showing the importance of anthropogenic forcing in determining the warming trend over the United States during the second half of the twentieth century (Hegerl et al. 2007).² Figures 11a and 11b show that the observed area-mean annual mean warming trend over

the United States during 1950–2000 is, indeed, mainly forced by the GW SST EOF, with the PDV SST EOF and the residual SST component contributing to a cooling trend. In contrast, the observed increasing area mean annual mean precipitation trend over the central United States is mainly forced by the PDV SST EOF and the residual SST component, with the GW EOF forcing a dry annual mean response. The contrast between the third bar and the seventh bar in Figs. 11a and 11b shows the extent to which the sum of the responses to the individual forcing terms disagrees with the response to the total trend forcing, that is, a measure of the nonlinearity in the responses. The nonlinearity in the responses has been tested to be statistically insignificant for both U.S. mean surface air temperature and central U.S. mean precipitation (not shown), and does not affect our main conclusions.

As a further comparison between our results and those from the IPCC AR4, we show in Figs. 11c and 11d the seasonality of the surface air temperature and precipitation trends over the period 1950–99 from the 66 coupled simulations of the climate of the twentieth century (20C3M, see Table 2) runs of the IPCC AR4 along with those from the CRU TS2.1 data and the NSIPP-1 AMIP ensemble mean. Note that the choice of 1950–99 instead of 1950–2000 for the 20C3M runs is because the former is the period when all 20C3M runs have data available. The results show a considerable spread among the various 20C3M ensemble members for both surface temperature and precipitation trends. While the annual-mean temperature trend of the 20C3M runs is clearly positive, most of the runs tend to simulate the strongest warming trend during late summer and early fall. This is in contrast with the observations and the AMIP ensemble mean simulations, which show the strongest warming trend in winter and a moderate cooling trend in late summer and fall. We note that the observed precipitation trend over the central United States is within the spread of the 20C3M runs throughout the seasonal cycle (Fig. 11d). In addition, in contrast with the NSIPP-1 AMIP ensemble mean, the ensemble mean of the 66 20C3M runs shows considerable warming trends and rather weak precipitation trends for all seasons, with the strongest warming trend and weak drying trends occurring in late summer and early fall.

The absence of the observed cooling trend in late summer and fall in the 20C3M runs is not surprising in view of our findings. Although some of the current generation of coupled general circulation models are capable of simulating realistic PDV (Solomon et al. 2007), these models need to reproduce the temporal phasing of the observed decadal variability during 1950–2000 in order to reproduce the observed seasonality and regionality of

² We note that, while emphasizing the importance of changes in SST, our study does not rule out other factors not considered here, including the direct effect of changing greenhouse gases, aerosols, and land use change as potential contributors to the seasonality and regionality of the U.S. climate trends.

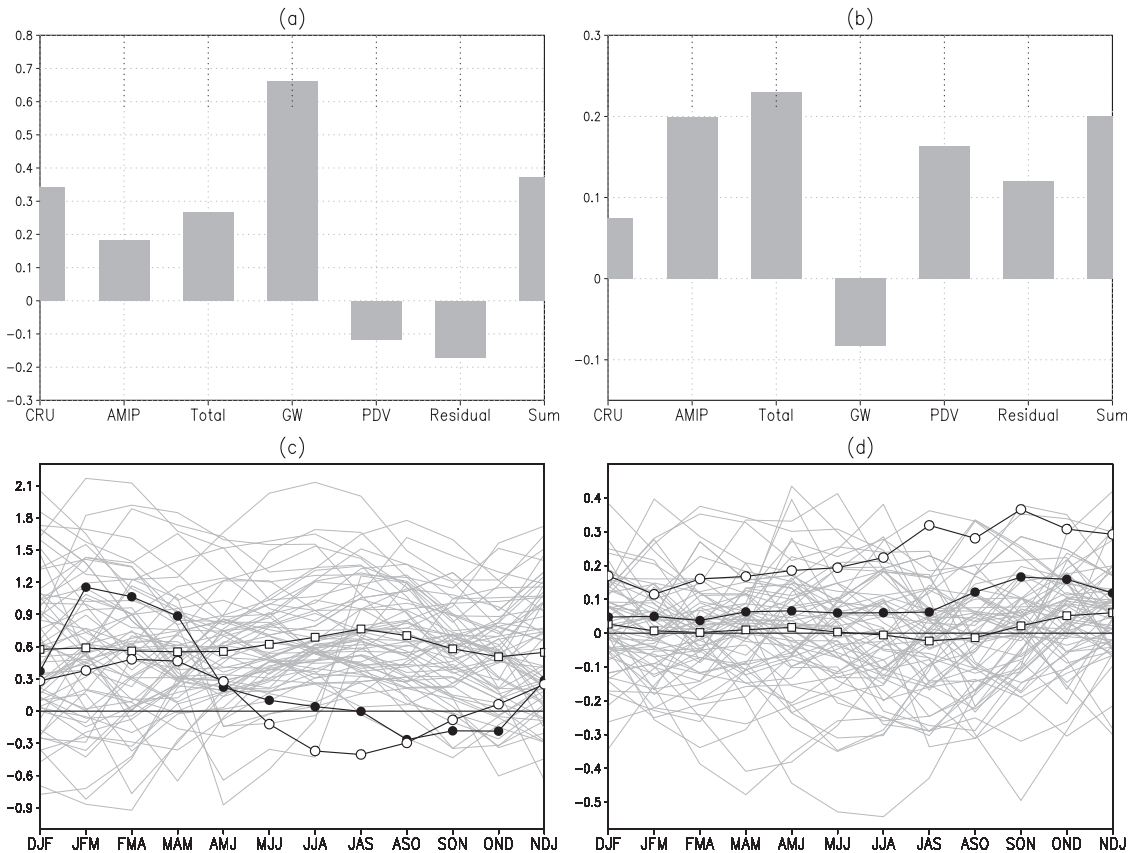


FIG. 11. Regional average of linear trends of (a) annual-mean surface air temperature (K) over the United States and (b) annual-mean precipitation (mm day^{-1}) over the central United States for the CRU TS2.1 observations, the NSIPP-1 AMIP ensemble mean simulation, the AGCM responses to the total SST trend, the GW SST EOF, the DV SST EOF, the residual SST component, and the sum of the AGCM responses to the GW SST EOF, the DV SST EOF, and the residual SST; regional average of linear trend of (c) surface air temperature over the United States and (d) precipitation over the central United States during 1950–99 for 66 20C3M individual runs (thin gray lines), the 66 20C3M ensemble mean (black line with open square), the CRU TS2.1 observations (black line with close circle), and the NSIPP-1 AMIP ensemble mean simulation (black line with open circle), for twelve 3-month running mean.

the U.S. climate trends during that period. Given the substantial internal variability and the fact that the 20C3M runs were not initialized with the observed atmospheric, land, and especially ocean states, it appears unlikely that they would be able to reproduce the temporal phasing of the observed PDV.

This study suggests that the climate trends over the United States may be viewed as a superposition of influences from decadal variability and global warming. The decadal variability alternately weakens and exaggerates the effect due to the anthropogenic warming. For the period 1950–2000, the phase changes of the PDV and the multidecadal variability in the Atlantic in the 1970s significantly contribute to the cooling and wetting trends over the central United States in the summer and fall months, whereas the global warming contributes to warming and drying. Over the central

United States, the effects of the former overwhelm that of the latter, resulting in the observed net cooling and wetting trends in that region. Thus, it appears that the climate over the central United States during 1950–2000 was controlled more by decadal variability than by global warming. The results also explain why the climate trends over the central United States, particularly that of the surface temperature, differ from that of the global mean as well as those over other continents where the impact of global warming appears to be more robust.

This study implies that, in the future, when the leading patterns of decadal to multidecadal variability in the Pacific and Atlantic are in their negative and positive phases, respectively, they could lead to warming and drying trends over the central United States during summer and fall. This, in combination with global

TABLE 2. List of IPCC AR4 CMIP3 20C3M model runs analyzed here. The IPCC AR4 coupled simulations of the climate of the twentieth-century experiment are driven by external historical forcings, designated as “20C3M” runs in the World Climate Research Program’s (WCRP’s) Coupled Model Intercomparison Project Phase 3 (CMIP3) data archive.

Model run	Model	Model indicators	Model run	References
1–5	Canadian Centre for Climate Modelling and Analysis (CCCma) Coupled General Circulation Model, version 3.1 (T47) resolution [CGCM3.1(T47)]	cccma_cgcm3_1	1–5	Kim et al. (2002)
6	CGCM3.1 (T63) resolution [CGCM3.1 (T63)]	cccma_cgcm3_1_t63	1	Kim et al. (2002)
7	Centre National de Recherches Météorologiques Coupled Global Climate Model, version 3 (CNRM-CM3)	cnrm_cm3	1	Salas-Mélia et al. (2005)
8–10	Commonwealth Scientific and Industrial Research Organisation Mark version 3.0 (CSIRO Mk3.0)	csiro_mk3_0	1–3	Gordon et al. (2002)
11	CSIRO Mark version 3.5 (CSIRO Mk3.5)	csiro_mk3_5	1	Gordon et al. (2002)
12–14	GFDL Climate Model version 2.0 (CM2.0)	gfdl_cm2_0	1–3	Delworth et al. (2006)
15–17	GFDL CM version 2.1 (CM2.1)	gfdl_cm2_1	1–3	Delworth et al. (2006)
18–19	GISS Atmosphere–Ocean Model (GISS-AOM)	giss_aom	1–2	Russell et al. (1995)
20–24	GISS Model E-H (GISS-EH)	giss_model_e_h	1–5	Schmidt et al. (2006)
25–33	GISS Model E-R (GISS-ER)	giss_model_e_r	1–9	Schmidt et al. (2006)
34–36	Flexible Global Ocean–Atmosphere–Land System Model gridpoint version 1.0 (FGOALS-g1.0)	iap_fgoals1_0_g	1–3	Yu et al. (2004)
37	Institute of Numerical Mathematics Coupled Model, version 3.0 (INM-CM3.0)	inmcm3_0	1	Volodin and Diansky (2004)
38	L’Institut Pierre-Simon Laplace Coupled Model, version 4 (IPSL CM4)	ipsl_cm4	1	Marti et al. (2005)
39	Model for Interdisciplinary Research on Climate 3.2, high-resolution version [MIROC3.2(hires)]	miroc3_2_hires	1	Hasumi and Emori (2004)
40–42	MIROC3.2, medium-resolution version [MIROC3.2(medres)]	miroc3_2_medres	1–3	Hasumi and Emori (2004)
43–45	ECHAM5/Max Planck Institute Ocean Model (MPI-OM)	mpi_echam5	1–3	Jungclaus et al. (2005)
46–50	Meteorological Research Institute Coupled General Circulation Model, version 2.3.2a (MRI CGCM2.3.2)	mri_cgcm2_3_2a	1–5	Yukimoto et al. (2001)
51–58	Community Climate System Model, version 3 (CCSM3)	ncar_ccsm3_0	1–7,9	Collins et al. (2006)
59–62	Parallel Climate Model (PCM)	ncar_cpm1	1–4	Washington et al. (2000)
63–64	Third climate configuration of the Met Office Unified Model (HadCM3)	ukmo_hadcm3	1–2	Gordon et al. (2000)
65–66	Hadley Centre Global Environmental Model version 1 (HadGEM1)	ukmo_hadgem1	1–2	Johns et al. (2004)

warming, could result in even stronger warming and drying trends over the United States, and thus more frequent heat waves and drought events during summer and fall.

Acknowledgments. This study is supported by the NASA Modeling, Analysis, and Prediction (MAP) project on Climate Transitions in the 1970s. We wish to acknowledge the international modeling groups for providing their data for analysis, the Program for Climate Model Diagnosis and Intercomparison (PCMDI)

for collecting and archiving the model data, the JSC/CLIVAR WGCM and their Coupled Model Intercomparison Project (CMIP) and Climate Simulation Panel for organizing the model data analysis activity, and the IPCC WG1 TSU for technical support. The IPCC Data Archive at Lawrence Livermore National Laboratory is supported by the Office of Science, U.S. Department of Energy. We thank two anonymous reviewers for their constructive comments and suggestions, which led to many improvements in the presentation of the results.

REFERENCES

- Bacmeister, J., P. J. Pegion, S. D. Schubert, and M. J. Suarez, 2000: Atlas of seasonal means simulated by the NSIPP 1 Atmospheric GCM. NASA Tech. Memo. 104606, Vol. 17, 194 pp.
- Chen, J., A. D. Del Genio, B. E. Carlson, and M. G. Bosilovich, 2008a: The spatiotemporal structure of twentieth-century climate variations in observations and reanalyses. Part I: Long-term trend. *J. Climate*, **21**, 2611–2633.
- , —, —, and —, 2008b: The spatiotemporal structure of twentieth-century climate variations in observations and reanalyses. Part II: Pacific pan-decadal variability. *J. Climate*, **21**, 2634–2650.
- Chou, M.-D., and M. J. Suarez, 1994: An efficient thermal infrared radiation parameterization for use in general circulation models. NASA Tech. Memo. 104606, Vol. 3, 85 pp.
- , and —, 2000: A solar radiation parameterization for atmospheric studies. NASA Tech. Memo. 104606, Vol. 11, 40 pp.
- Collins, W. D., and Coauthors, 2006: The Community Climate System Model version 3 (CCSM3). *J. Climate*, **19**, 2122–2143.
- Delworth, T. L., and Coauthors, 2006: GFDL's CM2 global coupled climate models. Part I: Formulation and simulation characteristics. *J. Climate*, **19**, 643–674.
- Enfield, D., A. M. Mestas-Núñez, and P. J. Trimble, 2001: The Atlantic multidecadal oscillation and its relation to rainfall and river flows in the continental U.S. *Geophys. Res. Lett.*, **28**, 2077–2080.
- Gordon, C., C. Cooper, C. A. Senior, H. T. Banks, J. M. Gregory, T. C. Johns, J. F. B. Mitchell, and R. A. Wood, 2000: The simulation of SST, sea ice extents and ocean heat transports in a version of the Hadley Centre coupled model without flux adjustments. *Climate Dyn.*, **16**, 147–168.
- Gordon, H. B., and Coauthors, 2002: The CSIRO Mk3 climate system model. CSIRO Atmospheric Research Tech. Paper 60, 134 pp. [Available online at http://www.cmar.csiro.au/e-print/open/gordon_2002a.pdf.]
- Hasumi, H., and S. Emori, Eds., 2004: K-1 coupled GCM (MIROC) description. K-1 Tech. Rep. 1, 39 pp.
- Hegerl, G. C., and Coauthors, 2007: Understanding and attributing climate change. *Climate Change 2007: The Physical Science Basis*, S. Solomon et al., Eds., Cambridge University Press, 663–745.
- Houghton, J. T., Y. Ding, D. J. Griggs, M. Noguer, P. J. van der Linden, X. Dai, K. Maskell, and C. A. Johnson, Eds., 2001: *Climate Change 2001: The Scientific Basis*. Cambridge University Press, 881 pp.
- Johns, T., and Coauthors, 2004: HadGEM1—Model description and analysis of preliminary experiments for the IPCC Fourth Assessment Report. Hadley Centre Tech. Note 55, 75 pp.
- Junglaus, J. H., and Coauthors, 2005: Ocean circulation and tropical variability in the coupled model ECHAM5/MPI-OM. *J. Climate*, **19**, 3952–3972.
- Kiehl, J. T., J. J. Hack, G. B. Bonan, B. A. Boville, D. L. Williamson, and P. J. Rasch, 1998: The National Center for Atmospheric Research Community Climate Model: CCM3. *J. Climate*, **11**, 1131–1149.
- Kim, S.-J., G. M. Flato, G. J. Boer, and N. A. McFarlane, 2002: A coupled climate model simulation of the last glacial maximum, Part 1: Transient multi-decadal response. *Climate Dyn.*, **19**, 515–537.
- Koster, R. D., and M. J. Suarez, 1996: Energy and water balance calculations in the Mosaic LSM. NASA Tech. Memo. 104606, Vol. 9, 194 pp.
- Kunkel, K. E., X.-Z. Liang, J. Zhu, and Y. Lin, 2006: Can CGCMs simulate the twentieth-century “warming hole” in the central United States? *J. Climate*, **19**, 4137–4153.
- Lee, M.-I., S. D. Schubert, M. J. Suarez, T. L. Bell, and K.-M. Kim, 2007: Diurnal cycle of precipitation in the NASA Seasonal to Interannual Prediction Project atmospheric general circulation model. *J. Geophys. Res.*, **112**, D16111, doi:10.1029/2006JD008346.
- Louis, J.-F., M. Tiedtke, and J.-F. Geleyn, 1981: A short history of the PBL parameterisation at ECMWF. *Proc. ECMWF Workshop on Planetary Boundary Layer Parameterisation*, Reading, United Kingdom, ECMWF, 59–80.
- Marti, O., and Coauthors, 2005: The new IPSL climate system model: IPSL-CM4. Institut Pierre Simon Laplace des Sciences de l'Environnement Global Tech. Rep., 101 pp.
- Mitchell, T. D., and P. D. Jones, 2005: An improved method of constructing a database of monthly climate observations and associated high-resolution grids. *Int. J. Climatol.*, **25**, 693–712.
- Moorthi, S., and M. Suarez, 1992: Relaxed Arakawa–Schubert: A parameterization of moist convection for general circulation models. *Mon. Wea. Rev.*, **120**, 978–1002.
- Pan, Z., R. W. Arritt, E. S. Takle, W. J. Gutowski Jr., C. J. Anderson, and M. Segal, 2004: Altered hydrologic feedback in a warming climate introduces a “warming hole.” *Geophys. Res. Lett.*, **31**, L17109, doi:10.1029/2004GL020528.
- Pegion, P., S. Schubert, and M. J. Suarez, 2000: An assessment of the predictability of northern winter seasonal means with the NSIPP 1 AGCM. NASA Tech. Memo. 104606, Vol. 18, 100 pp.
- Rayner, N. A., D. E. Parker, E. B. Horton, C. K. Folland, L. V. Alexander, D. P. Rowell, E. C. Kent, and A. Kaplan, 2003: Global analyses of sea surface temperature, sea ice, and night marine air temperature since the late nineteenth century. *J. Geophys. Res.*, **108**, 4407, doi:10.1029/2002JD002670.
- Robinson, W. A., R. Ruedy, and J. E. Hansen, 2002: General circulation model simulations of recent cooling in the east-central United States. *J. Geophys. Res.*, **107**, 4748, doi:10.1029/2001JD001577.
- Russell, G. L., J. R. Miller, and D. Rind, 1995: A coupled atmosphere-ocean model for transient climate change studies. *Atmos.–Ocean*, **33**, 683–730.
- Salas-Méllia, D., and Coauthors, 2005: Description and validation of the CNRM-CM3 global coupled model. CNRM Working Note 103, 36 pp.
- Schmidt, G. A., and Coauthors, 2006: Present-day atmospheric simulations using GISS ModelE: Comparison to in situ, satellite, and reanalysis data. *J. Climate*, **19**, 153–192.
- Schubert, S. D., M. J. Suarez, P. J. Pegion, M. A. Kistler, and A. Kumar, 2002: Predictability of zonal means during boreal summer. *J. Climate*, **15**, 420–434.
- , —, —, R. D. Koster, and J. T. Bacmeister, 2004: Causes of long-term drought in the U.S. Great Plains. *J. Climate*, **17**, 485–503.
- Seager, R., Y. Kushnir, C. Herweijer, N. Naik, and J. Velez, 2005: Modeling of tropical forcing of persistent droughts and pluvials over western North America: 1856–2000. *J. Climate*, **18**, 4065–4088.
- Solomon, S., D. Qin, M. Manning, M. Marquis, K. Averyt, M. M. B. Tignor, H. L. Miller Jr., and Z. Chen, Eds., 2007: *Climate Change 2007: The Physical Science Basis*. Cambridge University Press, 996 pp.

- Suarez, M. J., and L. L. Takacs, 1995: Documentation of the ARIES/GEOS Dynamical Core, version 2. NASA Tech. Memo. 104606, Vol. 5, 56 pp.
- Volodin, E. M., and N. A. Diansky, 2004: El Niño reproduction in coupled general circulation model of atmosphere and ocean. *Russ. Meteor. Hydrol.*, **12**, 5–14.
- Washington, W. M., and Coauthors, 2000: Parallel climate model (PCM) control and transient simulations. *Climate Dyn.*, **16**, 755–774.
- Yu, Y., X. Zhang, and Y. Guo, 2004: Global coupled ocean-atmosphere general circulation models in LASG/IAP. *Adv. Atmos. Sci.*, **21**, 444–455.
- Yukimoto, S., and Coauthors, 2001: The New Meteorological Research Institute coupled GCM (MRI-CGCM2): Model climate and variability. *Pap. Meteor. Geophys.*, **51**, 47–88.
- Zhang, Y., J. M. Wallace, and D. S. Battisti, 1997: ENSO-like interdecadal variability: 1900–93. *J. Climate*, **10**, 1004–1020.